Reprinted from The Journal of Physical Chemistry, 1993, 97.

Physical Chemistry of the H_2SO_4/H_2O Binary System at Low Temperatures: Stratospheric Implications

Renyi Zhang, Paul J. Wooldridge, Jonathan P. D. Abbatt,† and Mario J. Molina*

Department of Earth, Atmospheric and Planetary Sciences and Department of Chemistry, Massachusetts Institute of Technology, Cambridge, Massachusetts 02139

Received: February 19, 1993; In Final Form: April 21, 1993

Laboratory experiments have been carried out to investigate the physical chemistry of the H_2SO_4/H_2O binary system under conditions characteristic of the stratosphere. Water vapor pressures of sulfuric acid solutions (20–70 wt %) and of liquid–solid and solid–solid phase coexistence systems have been measured by mass spectrometry at temperatures between 190 and 240 K. Infrared spectra of the liquid, supercooled liquid, and crystalline hydrates of this system have also been investigated. The results indicate that some of the hydrates of sulfuric acid (i.e., $H_2SO_4 \cdot 4H_2O$, $H_2SO_4 \cdot 6.5H_2O$, and $H_2SO_4 \cdot 8H_2O$) may form and persist under the temperature and water partial pressure conditions typical of the high-latitude stratosphere.

Introduction

The stratospheric background aerosol layer, which exists at altitudes between about 10 and 25 km, consists mainly of particles of aqueous sulfuric acid with a mean diameter of ~ 0.1 μm and a concentration from 1 to 10 cm^{-3}.[1] Major volcanic eruptions, such as the 1991 eruption of Mt. Pinatubo, may increase the background concentration by more than an order of magnitude. Recent interest in stratospheric aerosols has focused on their role in the occurrence of the Antarctic ozone "hole" as well as in global ozone loss, through heterogeneous chemical processes. These background sulfate aerosols are important in heterogeneous chemistry for at least two reasons: (1) they may act as nuclei for the formation of polar stratospheric clouds (PSCs);[2-5] and (2) they may participate directly in heterogeneous reactions involving $ClONO_2$, HCl, N_2O_5, and H_2O to promote the release of active chlorine and to affect the stratospheric NO_x budget.[6-11]

A number of authors[12-18] have investigated the melting points and phase equilibria of the sulfuric acid/water binary system, establishing the existence of several crystalline hydrates, namely mono-, di-, tri-, tetra-, hemihexa-, and octahydrate. Giauque *et al.*[16] reported chemical potentials and various other thermodynamic properties of aqueous sulfuric acid solutions and crystalline hydrates, and their results were used by Gmitro and Vermeulen[19] and by Jaecker-Voirol *et al.*[20,21] to calculate vapor pressures of water and sulfuric acid. Recently, a more comprehensive summary of thermodynamic properties of the aqueous sulfuric acid system has been reported by Zeleznik.[22] In addition, a number of spectroscopic studies have been carried out for this binary system.[23-25]

At present, however, assessments of the role of sulfuric acid aerosols in the formation of PSCs and in promoting heterogeneous chemistry are still limited by the lack of reliable knowledge of thermodynamic properties of the H_2SO_4/H_2O binary system under conditions characteristic of the stratosphere. For example, no direct measurements have been made of vapor pressures for liquid and supercooled solutions at stratospheric temperatures; such measurements are needed in order to verify the earlier theoretical predictions.

In this paper we report vapor pressure measurements of the H_2SO_4/H_2O bnary system for liquid solutions, as well as for the liquid–solid and solid–solid coexistence systems involving some of the crystalline hydrates. Also, we report infrared spectra of sulfuric acid for liquid solutions and for various hydrates, showing the degree of dissociation of H_2SO_4 in the liquids and the unique spectral signatures of the individual crystals. In a separate paper we present vapor pressure measurements of the ternary liquid systems $H_2SO_4/HNO_3/H_2O$ and $H_2SO_4/HCl/H_2O$;[5] in another paper we discuss our investigations on the solid–liquid and solid–solid equilibria for these ternary systems as well as stratospheric implications in terms of the mechanism of formation of PSCs and of their role in heterogeneous chemistry.[26]

Experimental Section

Vapor Pressure Measurements. The apparatus has been described by Zhang *et al.*;[5] briefly, it consisted of a glass vessel where the liquid sample resided and where equilibrium with the gas phase was established, a gas-handling line for H_2O, pressure and temperature sensors, and a mass spectrometer for gas analysis. The cold region in the sample vessel was 3–4 cm high and 6 cm in diameter. The temperature of the sample was monitored by a thermocouple attached to the exterior of the vessel and was regulated by a combination of liquid nitrogen cooling and resistive heating to ±0.1 °C. Inside the sample vessel, a magnetic bar enclosed in glass was used to stir the liquid in order to ensure a homogeneous composition.

Vapor samples were drawn through a jacketed tube kept at room temperature by circulating water. A glass vacuum line fed the gas samples to the mass spectrometer though an orifice about 0.2 cm in diameter. The H_2O vapor pressures were calibrated using literature values for pure ice.[27] The effect of thermal transpiration along the transition to the room temperature vacuum line was taken into account as described by Hanson and Mauersberger.[28] The experimental detection limit for mass 18 was near $\sim 10^{-5}$ Torr. At each concentration vapor pressure measurements were performed at least twice and the data exhibited in general excellent reproducibility. The estimated error limits of our vapor pressure data are about ±10%, considering temperature, background signal and calibration uncertainties.

Infrared Spectra. Figure 1 shows schematically the apparatus used for infrared spectroscopic studies. The samples were prepared by placing a drop of bulk solution between infrared transmitting windows (discs of AgCl or ZnSe) and then pressing the windows to spread the drop into a film of a few micrometers thickness. The backing plate for the windows was a temperature-controlled copper bar and the assembly was purged to prevent condensation. The temperature calibration of the system was verified by observing the phase transition of a cyclohexane film at 186 K. Data was acquired using a Nicolet 800 Fourier transform spectrometer at 2 cm^{-1} resolution.

† Current address: Department of Geophysical Sciences, University of Chicago, Chicago, IL 60637.

0022-3654/93/2097-7351$04.00/0

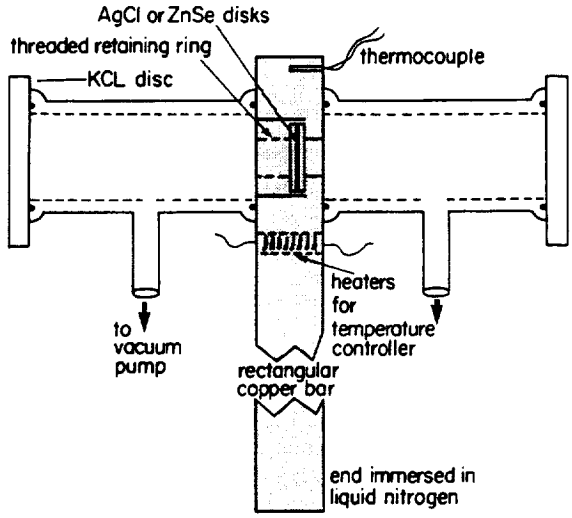

Figure 1. Schematic diagram of the cell used for infrared transmission measurements.

TABLE I: Coefficients from a Least-Squares Fit of log P_w = $A - B/T$ for Water Vapor Pressures[a]

wt % H_2SO_4	A	B
33.85	9.735	2514
35.7	9.674	2496
37.5	9.523	2485
44.2	9.268	2488
56.6	9.466	2623
62.6	9.543	2710
67.8	9.479	2785
70.0	9.710	2831
tetra-/dihydrate coexistence	11.502	3236

[a] P_w, Torr; T, kelvin.

Thermal Analysis and Sample Preparation. Thermal analysis was performed by differential scanning calorimetry (DSC), using a commercial calorimeter (Perkin-Elmer DSC-7). Titanium or gold plated capsules were used to hold the solutions.

Bulk liquid mixtures were prepared by diluting 95.6 wt % sulfuric acid solutions with distilled water. The liquid compositions were analyzed either by standard acid-based titration or by density measurements at room temperature. The accuracy of both methods was about ±0.1 wt %. Typically, 3 cm^3 of liquid was used for the vapor pressure measurements, while less than 0.03 cm^3 was employed for infrared spectroscopy and thermal analysis. For the vapor pressure measurements, the liquid compositions were analyzed before and after each experiment.

Results and Discussion

Vapor Pressure Measurements. *Liquid and Supercooled Liquid.* H_2O vapor pressures, P_w, of liquid and supercooled sulfuric acid solutions were measured for H_2SO_4 contents ranging from 20 to 70 wt %. Coefficients of the least squares fits in the form of log $P_w = A - B/T$ for the cases investigated here are summarized in Table I. Figure 2 shows the Clausius–Clapeyron plot for some selected H_2SO_4 concentrations: the open circles label experimental data points and the solid lines are the least-squares fits to the data. As shown in the figure, over the relatively narrow temperature range investigated the temperature dependence of the H_2O vapor pressures for a given composition is well described by the linear equation. This observation is consistent with our earlier report,[5] where we discuss limitations of the linear fits for extrapolations over a wide temperature range.

The dashed-dotted lines in Figure 2 represent the estimates based on the work of Jaecker-Voirol *et al.*[20,21] and the dashed lines based on that of Gmitro and Vermeulen.[19] Both sets of data were derived from thermodynamic measurements other than vapor

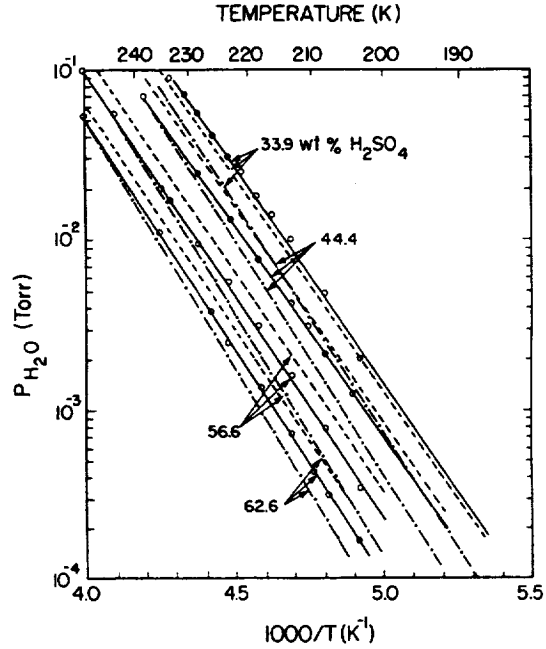

Figure 2. Water vapor pressures of liquid and supercooled liquid. Weight percentages of H_2SO_4 are labeled in the figure. The solid lines are the least-squares fits of the experimental data (open circles) from this work. The dashed-dotted lines are data taken from Jaecker-Voirol *et al.*,[20,21] and the dashed lines from Gmitro and Vermeulen.[19]

pressures and are in poor agreement with our measurements for the more concentrated solutions (~60 wt %); in the first set, the Clausius–Clapeyron equation was integrated assuming a constant heat capacity difference, whereas in the second set the heat capacity difference was linearized with temperature. In fact, the heat capacity of sulfuric acid solutions changes with temperature and composition in a complicated manner,[16,22] because of the occurrence of several ionization reactions, as discussed in the "Infrared Spectra" section. For the more dilute solutions (≤37 wt %) the results based on the report of Gmitro and Vermeulen are in reasonable agreement with our data, whereas those based on Jaecker-Voirol *et al.* yield significantly lower water vapor pressures. These lower values are clearly in error, because for such dilute solutions the H_2O vapor pressure can be predicted accurately at one particular temperature, namely at the equilibrium freezing point: the H_2O vapor pressure is practically the same as that of pure ice at that temperature. For those compositions the solid phase that is in equilibrium with the liquid at the freezing point is ice; consequently, the chemical potential of H_2O—and hence the H_2O vapor pressure—has the same value in those two phases. Furthermore, since the ice phase in consideration has only trace amounts of H_2SO_4, its H_2O chemical potential is essentially equal to that of pure ice. Within experimental error (i.e., within about 5%) this prediction was borne out by our measurements (see also Figure 4).

When extrapolated to room temperature, our vapor pressures agree well with literature values.[29] Vapor pressures over 68.4–85 wt % H_2SO_4 were also measured by Daudt[30] down to 220 K: his 68.4 wt % values fall essentially on the same line as our measurements. Also, as shown in Figure 3, our results are in good agreement with the H_2O vapor pressures calculated using the relative chemical potentials tabulated by Zeleznik[22] at 200 and 250 K (within 20%).

For convenience in presentation, our experimental water vapor pressures were fitted as a function of the H_2SO_4 concentration as follows

$$\log P_w = a_1 + a_2 w + a_3 w^2 + a_4 w^3 \qquad (1)$$

where w is the H_2SO_4 weight fraction (i.e., $w = 0.4$ for a 40 wt % solution). The coefficients a_i ($i = 1, 4$) are given in the form

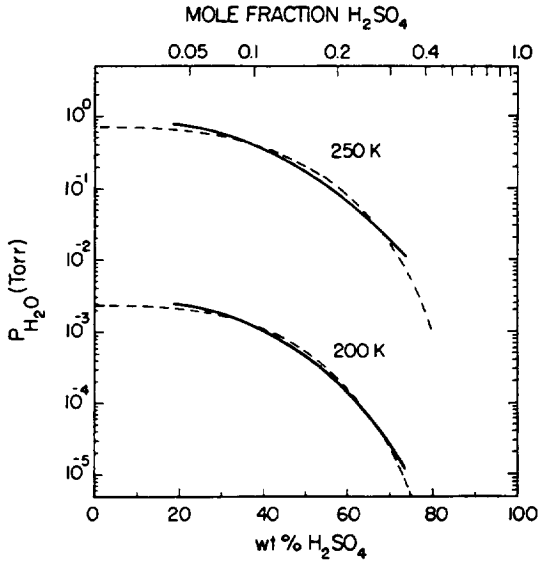

Figure 3. Water vapor pressures as a function of H_2SO_4 wt % at 200 and 250 K. The solid lines are results from this study, while the dashed lines are calculated using the tabulated relative chemical potentials reported by Zeleznik.[22]

TABLE II: Values of the Coefficients for Eq 1[a]

	A	$B \times 10^{-3}$
a_1	9.60	−2.44
a_2	4.04	−0.77
a_3	−16.82	3.19
a_4	16.03	−4.20

[a] $\log P_w = a_1 + a_2w + a_3w^2 + a_4w^3$. $a_i = A + B/T$ ($i = 1, 4$). P_w, Torr. T, kelvin.

of $a_i = A + B/T$ in Table II. In general, there is less than 10% difference between the values calculated using eq 1 and the experimental data. This expression is valid only for the acid concentration range employed in our measurements, i.e., from 20 to 70 wt % H_2SO_4.

Freezing Envelopes. According to the phase rule, the thermodynamic state for a three-phase equilibrium in a binary system is uniquely determined at a given temperature. The three phases can be a vapor and two solids, or a vapor, a liquid, and a solid. Hence, in a plot of temperature vs vapor pressure of one of the components the phase boundaries enclosing stability domains for the liquid or for the various hydrates can be represented as lines. The freezing envelopes are the boundaries between the stability domains for the liquid and solid phases. Vapor pressures and compositions of partially frozen equilibrium mixtures follow the freezing envelopes, a process that might continue at temperatures below the eutectic point (211 K for ice/hemihexahydrate) if the neighboring crystal phase does not nucleate, as we noted earlier for the HCl/H_2O system.[31]

The freezing envelopes inferred from our measurements are presented as solid curves in Figure 4, with the experimental points shown as open circles. For comparison, the freezing envelopes obtained by intersection of the vapor pressures reported by Jaecker-Voirol *et al.*[20,21] with the freezing points measured by Gable *et al.*[14] are presented as dashed curves. As pointed out above, there is a significant discrepancy along the phase boundary of the ice/liquid mixture between the H_2O vapor pressures measured in our study (which are very close to those of pure ice) and the estimates based on the work of Jaecker-Voirol *et al.*,[20,21] which yield much lower values.

Solids. The solid–liquid phase diagram for the H_2SO_4/H_2O binary system was investigated by Gable *et al.*[14] and by Vuillard.[15] These authors identified five hydrates: mono-, di-, tri-, tetra-, and hexahydrate. Hornung *et al.*[17] addressed the controversy related to the existence of another solid phase, the octahydrate;

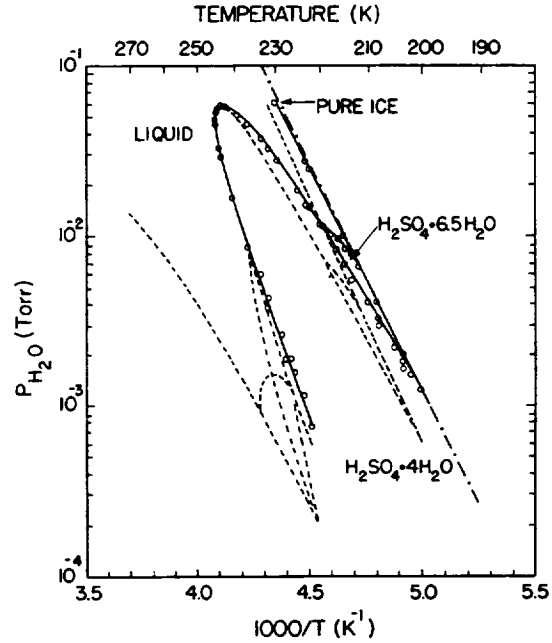

Figure 4. Water vapor pressures over partially frozen mixtures. The open circles and solid line are results from this study, while the dotted line is the intersections of the Jaecker-Voirol *et al.*[20,21] vapor pressure data with the freezing points reported by Gable *et al.*[14] The ice line is also plotted for reference.

additionally, they suggested that the proper stoichiometry for the "hexahydrate" is 13:2, and hence that it is actually an hemihexahydrate. Mootz and Merschenz-Quack[18] further corroborated these findings by providing structural data from powder X-ray crystallography.

We carried out vapor pressure measurements of the solid crystals in the same manner as those for the liquids (except, of course, that the solids were not stirred). As expected, thermodynamic equilibrium between bulk solids required much longer times to be established: in most cases several hours. Water vapor pressures were measured for the coexistence systems of ice/octahedrate or ice/tetrahydrate, ice/hemihexahydrate, and tetrahydrate/dihydrate. These results are presented in Figure 5 as squares, triangles, and crosses, respectively. The freezing envelopes determined from our measurements are plotted as dotted curves. Also shown in this figure are the vapor pressures for liquid solutions (dashed lines).

The experimental water vapor pressures of the coexistence mixtures lie on straight lines when plotted as $\log P_w$ vs. $1/T$. The scatter in the data about these lines is small (less than 5%), indicating that equilibrium between the two solid compounds was effectively achieved. As expected, the H_2O vapor pressures over the coexistence mixtures of ice/tetrahydrate, ice/octahydrate, and ice/hemihexahydrate were very near those of pure ice (to within 5%); the reason was discussed earlier. The results of a least squares fit of $\log P_w = A - B/T$ for the di/tetrahydrate coexistence mixture are given also in Table I.

By taking into account the fact that the vapor pressures for each of the two components are the same when two solid phases are in equilibrium, we derive the following equation for the slope of the coexistence line

$$B = -\left(\frac{\partial \log (P_w)}{\partial (1/T)}\right)_{coex} = -\frac{\Delta H_0 - \Delta H_0'}{2.3R(n - n')} \qquad (2)$$

where R is the gas constant, the primed quantities refer to the second hydrate, and ΔH_0 is the standard enthalpy change for the following process:

$$nH_2O(g) + H_2SO_4(g) \rightarrow H_2SO_4 \cdot nH_2O(s) \qquad (3)$$

Liquid-phase standard enthalpies of formation for tetrahydrate

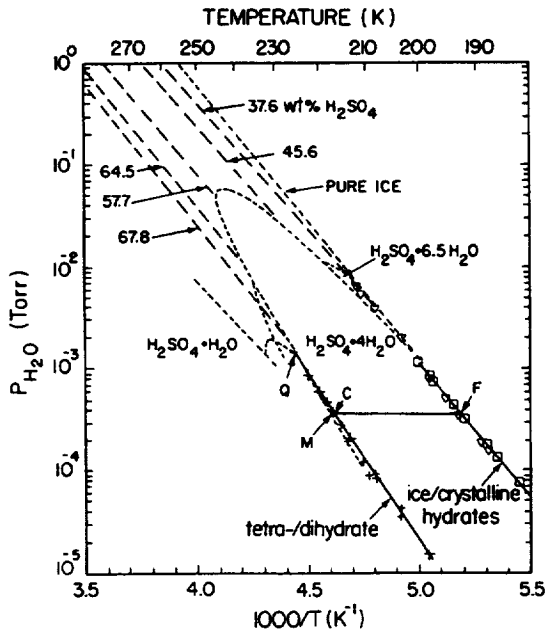

Figure 5. Vapor pressures of water for solids in the H_2SO_4/H_2O binary system: +, tetrahydrate/dihydrate; □, ice/tetrahydrate or ice/octahydrate; ▽, ice/hemihexahydrate. The coexistence lines and the freezing envelopes are labeled. The dashed lines are for H_2O vapor pressures of liquid solutions. The solid line F–C–M represent a warming process at a H_2O partial pressure of 3.8×10^{-4} Torr (corresponding to a mixing ratio of 5 ppmv at 100 mb, ~16 km altitude in the stratosphere). Point Q labels the quadruple point for H_2SO_4•2H_2O and H_2SO_4•4H_2O coexisting with the gas and the liquid phases.

and dihydrate and the enthalpies of fusion for these pure hydrates have been reported by Zeleznik;[22] based on that work, we estimate values of −2047 and −1454 kJ/mol for the standard enthalpies of formation at 200 K for the two solid phases. Using eq 2, along with the standard enthalpy of formation of water (−240.9 kJ/mol[32]), we derive a slope of 3022 K for the coexistence line of dihydrate and tetrahydrate, consistent with our measured value of 3236 K given in Table I.

As pointed out above, there is a unique relationship between the vapor pressure and the temperature for the equilibrium coexistence of two solid phases. Bulk solid mixtures often require a long time to reach equilibrium, but the use of small samples in some of the flow tube experiments facilitated this process. Experiments were performed using solutions with a H_2SO_4 concentration near that of the tetrahydrate: upon freezing, the solids exhibited initially H_2O vapor pressures very close to those of pure ice, characteristic of the coexistence mixture of ice/tetrahydrate. By slowly raising the temperature and by flowing dry helium over the samples, a sudden drop in the water vapor pressure was observed after some time, suggesting that the ice phase had evaporated, leaving only H_2SO_4•4H_2O behind. The equilibrium H_2O vapor pressures over the substrate could then be regulated simply by addition or evaporation of small amounts of water, keeping the temperature constant; that is, the "H_2SO_4-rich" and "H_2O-rich" forms of the tetrahydrate could be generated by controlling the H_2O vapor pressure. The lowest values of this vapor pressure attained by evaporation agreed closely with those of the di/tetrahydrate coexistence mixture measured using bulk samples. As the temperature was raised over a period of 5–10 min, final melting was observed to occur at 243 K, which corresponds to the melting point of pure tetrahydrate. These results are qualitatively similar to those obtained earlier with the HNO_3/H_2O system, in agreement with the expectations based on phase equilibria considerations.[33] In the same manner, the hemihexahydrate was generated by freezing a solution with a 13:2 stoichiometric ratio (45.6 wt % H_2SO_4). As before, the H_2O vapor pressures initially attained were close to those of pure ice, indicating the formation of an ice/hydrate equilibrium mixture. H_2O vapor pressures smaller than those of pure ice could be obtained by evaporating enough H_2O from this mixture to remove the ice phase, leaving the hydrate behind.

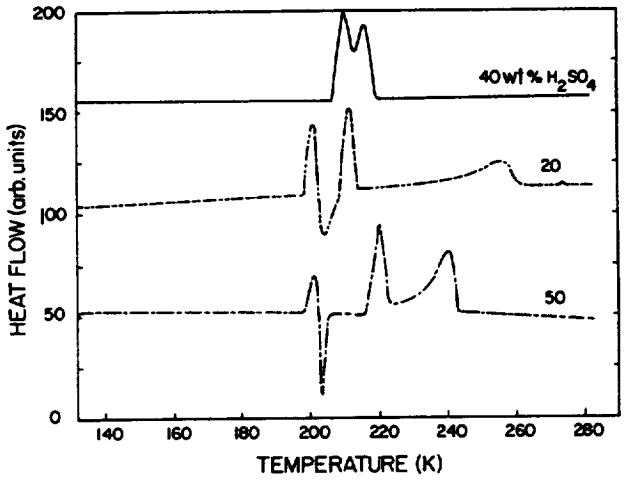

Figure 6. DSC warming curves showing hydrate meltings. The peaks near 200 K represent either the eutectic meltings of ice/tetrahydrate followed by crystallization into hemihexahydrate, or the solid to solid conversion of octahydrate into hemihexahydrate. The coexistence mixtures of ice/hemihexahydrate melt near 211 K. For the 50 wt % H_2SO_4 frozen mixture, the H_2SO_4•6.5H_2O undergoes a peritectic reaction at 219 K to form H_2SO_4•4H_2O. For the 20 wt % H_2SO_4 frozen mixture, the warmest peak corresponds the melting of ice. Weight percentages of H_2SO_4 are labeled in the figure.

Samples with sulfuric acid concentrations greater than about 60 wt % would usually not crystallize upon cooling, as noted also by Gable *et al.*[14] These authors also reported that the trihydrate did not form these solutions unless seeded with trihydrate crystals, but the dihydrate or tetrahydrate formed instead. By repeated cooling and warming between 150 and 210 K we were able to freeze the 60 wt % solutions in the sample vessel utilized for vapor pressure measurements: crystallization occurred upon warming near 200 K. The solid began to melt at 226 K and hence consisted of an equilibrium mixture of tetra- and dihydrate, in agreement with the observations of Gable *et al.*[14]

Some experiments were performed using the flow tube–mass spectrometer apparatus to investigate the melting behavior of solid H_2SO_4 aerosols in the stratosphere. H_2SO_4 tetrahydrate was first established by freezing the appropriate composition. Subsequently, the temperature of the sample was slowly raised, keeping the H_2O partial pressure constant. As is represented by the line F–C–M in Figure 5, this process involves the transformation of "H_2O-rich" to "H_2SO_4-rich" hydrate, accompanied by only a minor change in the bulk composition of the hydrate (we have described previously a similar process involving nitric acid trihydrate[33]). The sample was observed visually to melt at 218 K, corresponding to point M in Figure 5, which represents equilibrium between the tetrahydrate and the liquid at the particular H_2O partial pressure of the experiment. In principle, a solid–solid phase transition could have occurred at point C, the coexistence point between di- and tetrahydrate, if nuclei for the formation of the dihydrate had been present; if so, the sample would not have started to melt at point M. This result is analogous to that involving freezing envelopes discussed earlier: a solid and a liquid phase can be in thermodynamic equilibrium with each other under conditions where both are metastable with respect to a different solid phase.

Calorimetric Measurements. Figure 6 shows DSC warming curves of frozen sulfuric acid mixtures. The results show that the frozen sample of 20 wt % (middle curve) consists initially of a mixture of ice and octahydrate and that this hydrate transforms into the hemihexahydrate at 200 K. Upon further warming, the

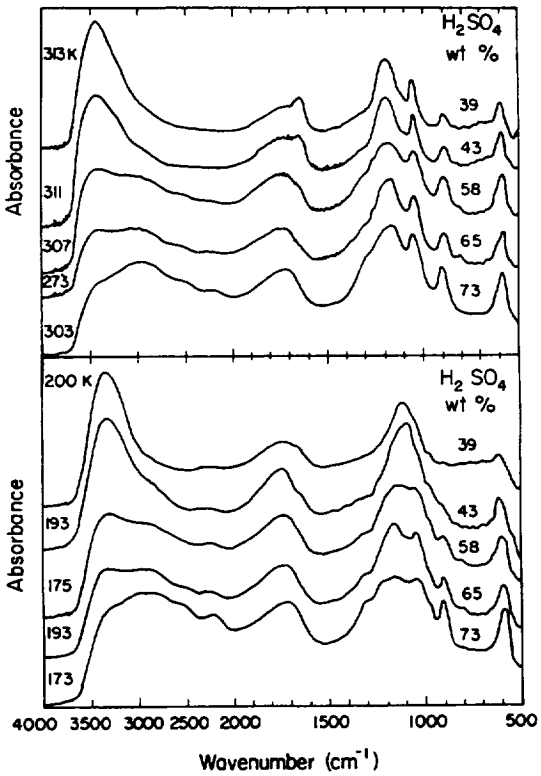

Figure 7. Infrared spectra of liquid H_2SO_4 solutions with compositions of 39, 43, 58, 65, and 73 wt % at temperatures near 300 and 190 K.

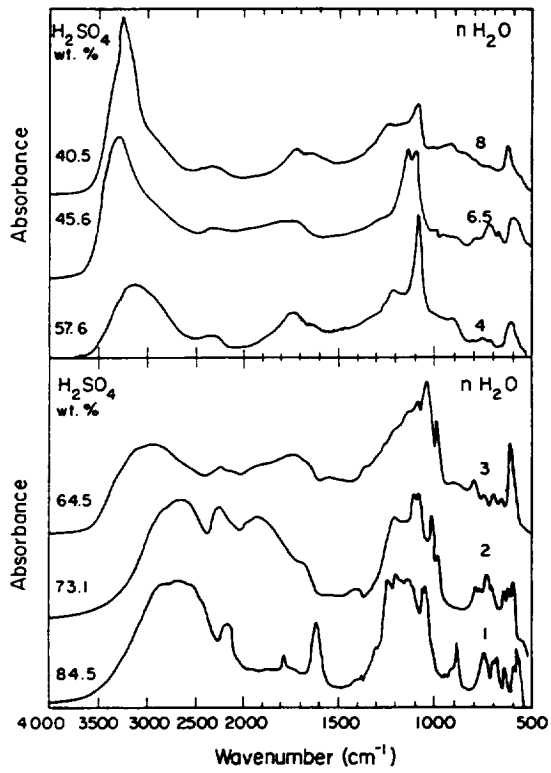

Figure 8. Spectra of crystalline hydrates $H_2SO_4 \cdot nH_2O$. For n = 1, 2, and 3 the spectra are presented at low temperatures (~140 K), showing sharper absorption bands. Spectra for n = 4, 6.5, and 8 change relatively little with temperature and are shown at 195 K.

hemihexahydrate melts at its eutectic with ice, 211 K, leaving ice and liquid. The last of ice melts at about 259 K. The frozen sulfuric acid solution of 50 wt % (bottom curve) consists initially a mixture of octahydrate and tetrahydrate; again, the octahydrate transforms into $H_2SO_4 \cdot 6.5H_2O$ at 200 K. However, the hemihexahydrate does not melt in this case; it undergoes a peritectic transition at 219 K to form the tetrahydrate. The sample with a content of 40 wt % (top curve) yields a coexistence mixture of ice and hemihexahydrate, with an eutectic point at 211 K and a final melting point around 217 K.

The phase transitions in Figure 6 correspond closely to those in the H_2SO_4 phase diagram reported by Giauque *et al.*[17] These results along with various other calorimetric measurements performed in our laboratory are in excellent agreement with the findings of Giauque *et al.*[17] and Mootz and Merschenz-Quack[18] in terms of establishing the nature of the phase diagram and the identity of the various hydrates.

Infrared Spectra. *Spectra of Liquid and Supercooled Liquid.* Figure 7 shows spectra of various supercooled liquid sulfuric acid solutions near room temperature and in the 170–200 K range. The spectra consist mainly of two regions: strong, very broad absorptions at frequencies higher than 1500 cm^{-1} arising from H_2O and H_3O^+ fundamentals, and somewhat narrower bands at lower frequencies, mostly from the sulfate group.

The bands in the spectra change slowly with temperature and composition and at room temperature are in good agreement with those reported by Palmer and Williams.[24] The spectra of the concentrated solutions undergo virtually no change in appearance with cooling, while for the more dilute solutions changes do occur. The changes are consistent with increased SO_4^{2-} at the expense of HSO_4^- upon cooling, by noting the band locations of SO_4^{2-} at 1104 and 613 cm^{-1} and HSO_4^- at 1341, 1230, 1050, 885, and 593 cm^{-1} summarized by Querry *et al.*[23] The increased ionization at lower temperatures was also observed in the Raman spectra of H_2SO_4 solutions by Dawson *et al.*[34] and by Kanno.[35] The marked shifting of $HSO_4^- \rightleftharpoons SO_4^{2-}$ results in the heat capacity changing in a complicated way, as noted earlier.

Spectra of Crystalline Sulfuric Acid Hydrates. Figure 8 shows the infrared spectra for various H_2SO_4 hydrates. Table III summarizes the frequencies of major infrared bands of these crystalline hydrates at temperatures around 140 K. Figure 9 illustrates the changes observed in the infrared spectra of a 47.6 wt % solution with temperature, showing the crystallization to form hemihexahydrate between 190 and 200 K, and the subsequent peritectic transition at 219 K to form the tetrahydrate, and melting at about 233 K. In general, for the pure crystalline hydrates, the melting points as well as phase transition temperatures agreed very well with those found in the thermal analysis and vapor pressure measurements.

Next, we discuss the spectra for each of the hydrates:

(*a*) *Monohydrate.* Our spectrum agrees very well with that reported by Savoie and Giguère[36] within the resolution and wavenumber accuracy of the earlier, non-FTIR work. The lack of symmetry of the bisulfate ion in the crystal[37] is consistent with the multitude of peaks in the spectrum, including the appearance of the sharp peak(s) in the 950–990-cm^{-1} range probably due to the symmetric sulfate ν_1 stretch,[34] which is infrared forbidden in a fully symmetric environment.

(*b*) *Dihydrate.* The spectrum reported by Giguère and Savoie[25] for the dihydrate is noticeably different from our crystalline spectrum but is similar to that of a supercooled film. Their sampling method was similar to ours, but, because of the lack of change in the bands, they expressed some doubt as to whether crystallization had indeed occurred. For genuinely crystalline samples, the X-ray structure[38] and Raman spectrum[39] show complete ionization, $(H_3O^+)_2SO_4^{2-}$. In an isotropic environment, the symmetric SO_4^{2-} group would have few observable infrared vibrations, but this crystal has two independent types of sulfate groups, neither of which are fully symmetric. Consequently, the complexity of the infrared spectrum here is also consistent with the reported structure.

(*c*) *Trihydrate.* No published structure or spectra are available for comparison, but the complexity of the spectrum indicates a low symmetry for the sulfate anion.

TABLE III: Frequencies (cm^{-1}) of Major Infrared Bands of Crystalline Hydrates of H_2SO_4 Sampled at 143 ± 10 K

$H_2SO_4 \cdot H_2O$	$H_2SO_4 \cdot 2H_2O$	$H_2SO_4 \cdot 3H_2O$	$H_2SO_4 \cdot 4H_2O$	$H_2SO_4 \cdot 6.5H_2O$	$H_2SO_4 \cdot 8H_2O$
3900–2500	2900–2550	3300–2700	3300–2800	3400–3150	3350–3100
2260–2100	2250	2250	2450–2250		2420–2200
1785	1925				
1616	1690	1950–1650	1725	1775	1720
1243					
1198	1204			1127	
1170					
1133		1131			
1114	1102				
1062	1078	1083	1077	1089	1079
1050	1013	1040			
947	989	988			
887	984				916
750	790	795			
696	767	746		709	
680	733	700			
644	710	650			
594	645	614		598	621
583	626				
574	598		600	562	

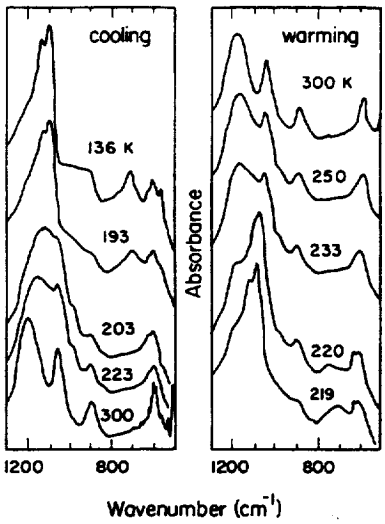

Figure 9. Evolution of infrared spectra of a 47.6 wt % H_2SO_4 solutions with temperatures. Crystallization of $H_2SO_4 \cdot 6.5H_2O$ occurs between 190 and 200 K upon cooling. No significant changes occur upon warming to 210 K. The hemihexahydrate converts into tetrahydrate plus liquid at around 220 K. The tetrahydrate melts by 233 K.

(*d*) *Tetrahydrate.* As with the dihydrate, the spectrum from Giguère and Savoie[25] strongly resembles that of a noncrystalline film, which is again noticeably different from the crystalline spectrum presented here. The spectrum consists of the broad H_3O^+ bands at higher frequencies and just two dominant SO_4^{2-} bands near 1077 and 600 cm^{-1} (for comparison, SO_4^{2-} in dilute potassium sulfate solution has active bands at 1104 and 613 cm^{-1}, according to Querry *et al.*[23]). This is consistent with the high symmetry of the ion in the crystal structure report.[40]

(*e*) *Hemihexahydrate.* Our results are consistent with the crystal structure report,[18] in that they showed a slightly distorted SO_4^{2-} ion with S–O distances nearly equal to those in the tetrahydrate. We also observed that around 220 K the hemihexahydrate converted into tetrahydrate plus some liquid (Figure 9), consistent with the DSC and vapor pressure measurements.

(*f*) *Octahydrate.* For this hydrate, the sulfate stretching region strongly resembles that of the tetrahydrate, which is reasonable considering the similarity of the reported site symmetries and bond lengths for the SO_4^{2-} ion in both crystals.[18] The spectral similarities, however, make differentiation between the pure octahydrate and a tetrahydrate/ice mixture difficult and hence there is some uncertainty in its identification. Here, the changes as the temperature is raised above the phase transition temperature do not lead to an unambiguous confirmation, because of the proximity of the octahydrate to hemihexahydrate transition at 201 K and the extrapolated ice–tetrahydrate metastable eutectic at 200 K.[16]

Stratospheric Implications

Sulfuric acid aerosols are hygroscopic and are essentially in equilibrium with water vapor in the stratosphere which is present at several ppm. In contrast, equilibrium with respect to H_2SO_4 vapor is less likely to be attained because of the exceedingly low concentrations of this vapor.[41] Equilibrium with water vapor implies that the stratospheric aerosol particles deliquesce as the temperature decreases. Steele *et al.*[42] estimated sulfuric acid concentrations as a function of temperature for a given ambient H_2O partial pressure, using the H_2O vapor pressure data taken from Gmitro and Vermeulen;[19] their results are shown in Figure 10, together with the estimates based on the data of Jaecker-Voirol *et al.*,[20,21] and with those based on our vapor pressure measurements. There is a significant disagreement between the curve estimated from the Jaecker-Voirol *et al.* data and the other two curves, as expected from our discussion in the "Vapor Pressure Measurements" subsection. Note, also, that below 200 K the aerosols contain significant amounts of nitric acid, which affects the H_2SO_4 concentrations.[5]

Figure 10 also shows freezing envelopes; as can be seen in the figure, the H_2SO_4 aerosols are supercooled for the conditions represented by the solid lines and are expected to be supercooled throughout most of the stratosphere. Atmospheric observations indicate that the bulk of the sulfate particles in the stratosphere are indeed in the liquid phase.[1,43–45] Supercooling experiments in our laboratory also indicate that the sulfate aerosols are not likely to freeze unless the temperature drops below ~200 K.[26]

If the temperature drops sufficiently, the aerosols may crystallize to form H_2SO_4 hemihexahydrate and/or tetrahydrate, together with HNO_3 trihydrate (NAT).[26] If the temperature reaches the frost point, ice may form as well (points F_a and F_b in Figure 10).

The situation with respect to the melting of frozen aerosols can be reasonably defined: once crystallized, the hydrates are stable until they either melt or evaporate. These are the processes for which the equivalent of supercooling does not occur, and hence, their occurrence can be predicted reliably using thermodynamic considerations. Consider, for example, a PSC particle consisting of NAT with a core of H_2SO_4 hemihexahydrate, in a region of the stratosphere that is warming. Above the saturation temperature with respect to NAT the bulk of the particle evaporates, leaving behind the hemihexahydrate; no melting occurs at this stage. This temperature is typically around 195–197 K, depending on the ambient partial pressures of HNO_3 and H_2O. Inspection

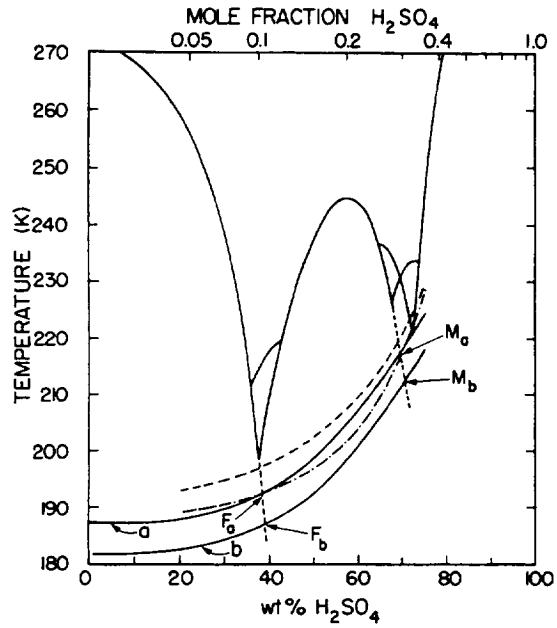

Figure 10. Equilibrium sulfuric acid compositions of background stratospheric aerosols as a function of temperature and H_2O mixing ratios at 100 mb (~16 km altitude), as estimated from different vapor pressure data: the solid lines are based on data from this work (*a*, 5 ppmv; *b*, 3 ppmv H_2O); the dashed line is based on data of Jaecker-Voirol *et al.*[20,21] (5 ppmv H_2O); the dashed-dotted line is from the results of Steele *et al.*[42] (5 ppmv H_2O). Also shown in this figure is the freezing envelop of sulfuric acid solutions.[14] Points *F* and *M* label the corresponding freezing and melting points.

of Figure 10 may lead, at first sight, to the conclusion that once frozen the sulfuric acid particle never melts in the stratosphere, because the temperatures characteristic of the region of stability of the liquid are not reached. However, this conclusion implies that solid–solid phase transformations do take place as the temperature increases. Our experiments show that indeed the hemihexahydrate as well as the octahydrate transform readily into the tetrahydrate, without melting. This process is likely to occur in the stratosphere as well and would be accompanied by evaporation of water. In contrast, our observations reveal that the tetrahydrate does not transform into any of the lower hydrates; instead it melts at a temperature at which it is in equilibrium with the liquid solution having a H_2O vapor pressure equal to the ambient H_2O partial pressure, typically around 215 K (point M in Figure 5 or points M_a and M_b in Figure 10). As melting occurs, water evaporates, because the liquid is more concentrated in H_2SO_4 than the tetrahydrate. Above this melting temperature the liquid phase is stable with respect to the tetrahydrate, although it is metastable with respect to the tri- and dihydrate. These two hydrates happen to be difficult to generate merely by cooling liquid solutions; they usually crystallize only after cooling below 150 K to form a glass, and after subsequent rewarming. As the temperature increases in the stratosphere the acid concentration increases, and at some point the liquid becomes metastable with respect to the monohydrate. However, crystallization of the sulfuric acid droplets does not appear to occur in the stratosphere at such temperatures, as inferred from atmospheric observations.[1,43-45]

We should point out, though, that sedimentation of ice crystals in late winter over Antarctic may remove a significant fraction of the frozen sulfate aerosols from the stratosphere, by scavenging[46] and by acting as condensation nuclei in the formation of PSCs.[2-5]

What are the consequences in terms of chlorine activation in the stratosphere? It is now clear that ice and NAT particles are very efficient in this respect.[47-49] Preliminary experiments in our laboratory indicate that chlorine activation also occurs readily on cold liquid sulfate aerosols, under conditions of supersaturation with respect to NAT formation in the stratosphere. Chlorine activation occurs as well on "water-rich" sulfuric acid tetrahydrate,[26] as is the case with "water-rich" NAT.[48] We are currently carrying out additional measurements to better quantify these heterogeneous processes and to establish the relative chlorine activation efficiency of the various condensed phases.

Conclusions

In this paper we have presented vapor pressure, DSC, and infrared spectroscopic measurements for liquid solutions and for various crystalline hydrates of sulfuric acid, in order to investigate the physical properties of background stratospheric sulfate aerosols. These measurements should be useful for laboratory studies simulating stratospheric aerosols. Furthermore, they indicate that crystalline sulfuric acid hydrates are important components of the stratospheric aerosol layer, particularly at high latitudes. Ongoing experiments in our laboratory indicate that these sulfate aerosols, in solid as well as in liquid form, can efficiently activate chlorine through heterogeneous processes at the low temperatures typical of the polar stratosphere in the winter and spring months. Hence, they are likely to play a direct role in ozone depletion similar to that of PSCs.

Acknowledgment. The authors are grateful to P. Hamill for sending a program to calculate vapor pressures based on the data of Gmitro and Vermeulen,[19] and to O. Toon for providing a preprint of their work. Helpful discussions with J. Dye are also greatly appreciated. This research was supported by an NSF grant (ATM-9017150) and a NASA grant (NAG2-632) to the Massachusetts Institute of Technology. R.Z. is supported by a NASA graduate fellowship and J.A. was supported by a NSERC (Canada) postdoctoral fellowship.

References and Notes

(1) Turco, R. P.; Whitten, R. C.; Toon, O. B. *Rev. Geophys.* **1982**, *20*, 233.
(2) Poole, L. R.; McCormick, M. P. *J. Geophys. Res.* **1987**, *93*, 8423.
(3) Hamill, P.; Turco, R. P.; Toon, O. B. *J. Atmos. Chem.* **1988**, *7*, 287.
(4) Wosfy, S. C.; Salawitch, R. J.; McElroy, M. B. *J. Atmos. Sci.* **1990**, *47*, 2004.
(5) Zhang, R.; Wooldridge, P. J.; Molina, M. J. *J. Phys. Chem.*, in press.
(6) Molina, M. J.; Tso, T.; Molina, L. T.; Wang, F. C. Y. *Science*, **1987**, *238*, 1253.
(7) Rodriguez, J. M.; Ko, M. K. W.; Sze, N. D. *Geophys. Res. Lett.* **1988**, *15*, 257.
(8) Tolbert, M. A.; Rossi, M. J.; Golden, D. M. *Geophys. Res. Lett.* **1988**, *15*, 847.
(9) Hofmann, D. J.; Solomon, S. *J. Geophys. Res.* **1989**, *94*, 5029.
(10) Wolff, E. W.; Mulvaney, R. *Geophys. Res. Lett.* **1991**, *18*, 1007.
(11) Hanson, D. R.; Ravishankara, A. R. *J. Geophys. Res.* **1991**, *96*, 17307.
(12) Pickering, S. U. *J. Chem. Soc.* **1890**, *57*, 331.
(13) Hulzmann, O.; Biltz, W. Z. *Anorg. Allg. Chem.* **1934**, *218*, 369.
(14) Gable, C. M.; Betz, H. F.; Maron, S. H. *J. Am. Chem. Soc.* **1950**, *72*, 1445.
(15) Vuillard, G. C. *Ann. Chim.* **1957**, *13*, 233.
(16) Giauque, W. F.; Hornung, E. W.; Kunzler, J. E.; Rubin, T. R. *J. Am. Chem. Soc.* **1960**, *82*, 62.
(17) Hornung, E. W.; Brackett, T. E.; Giauque, W. F. *J. Am. Chem. Soc.* **1956**, *78*, 5747.
(18) Mootz, D.; Merschenz-Quack, A. *Z. Naturforsch.* **1987**, *42b*, 1231.
(19) Gmitro, J. I.; Vermeulen, T. *AIChE J.*, **1964**, *10*, 740.
(20) Jaecker-Voirol, A.; Ponche, J. L.; Mirabel, P. *J. Geophys. Res.* **1990**, *95*, 11857.
(21) Jaecker-Voirol, A.; Ponche, J. L.; Mirabel, P. *J. Geophys. Res.* **1990**, *95*, 22565.
(22) Zeleznik, F. J. *J. Phys. Chem. Ref. Data* **1991**, *20*, 1157.
(23) Querry, M. R.; Waring, R. C.; Holland, W. E.; Earls, L. M.; Herrman, M. D.; Nijm, W. P.; Hale, G. M. *J. Opt. Soc. Am.* **1974**, *64*, 39.
(24) Palmer, K. F.; Williams, D. *Appl. Opt.* **1975**, *14*, 208.
(25) Giguère, P. A.; Savoie, R. *Can. J. Chem.* **1960**, *38*, 2467.
(26) Molina, M. J.; Zhang, R.; Wooldridge, P. J. To be submitted for publication.
(27) Jancso, G.; Pupezin, J.; Van Hook, W. A. *J. Phys. Chem.* **1970**, *74*, 2984.
(28) Hanson, D. R.; Mauersberger, K. *J. Phys. Chem.* **1988**, *92*, 6167.
(29) Hornung, E. W.; Giauque, W. F. *J. Am. Chem. Soc.* **1955**, *77*, 2744.

(30) Daudt, W. *Z. Phys. Chem.* **1923**, *106*, 255.
(31) Abbatt, J. P. D.; Beyer, K. D.; Fucaloro, A. F.; McMahon, J. R.; Wooldridge, P. J.; Zhang, R.; Molina, M. J. *J. Geophys. Res.* **1992**, *97*, 15819.
(32) Chase, M. W.; Davies, C. A.; Downey, J. R.; Frurip, D. J.; McDonald, R. A.; Syverud, A. N. *JANAF Thermodynamic Tables*; American Chemical Society: New York, 1985.
(33) Molina, M. J. *Chemistry of the Atmosphere: The impact of Global Change*. In *CHEMRAWN VII*; Calvert, J. G., Ed.; Blackwell Science: Oxford, U.K., in press.
(34) Dawson, B. S.; Irish, D. E.; Toogood, G. E. *J. Phys. Chem.* **1986**, *90*, 334.
(35) Kanno, H. *Chem. Phys. Lett.* **1990**, *170*, 382.
(36) Savoie, R.; Giguère, P. A. *J. Chem. Phys.* **1964**, *41*, 2298.
(37) Taesler, I.; Olovsson, I. *Acta Crystallogr.* **1968**, *B24*, 299.
(38) Taesler, I.; Olovsson, I. *J. Chem. Phys.* **1969**, *51*, 4213.
(39) Millen, D. J.; Vaal, E. G. *J. Chem. Soc.*, **1956**, 2913.
(40) Kjällman, T.; Olovsson, I. *Acta Crystallogr.* **1972**, *B28*, 1692.
(41) Möhler, O.; Arnold, F. *Ber. Bunsenges. Phys. Chem.* **1992**, *96*, 280.
(42) Steele, H. M.; Hamill, P.; McCormick, M. P.; Swissler, T. J. *J. Geophys. Res.* **1983**, *40*, 2055.
(43) Dye, J. E.; Baumgardner, D.; Gandrud, B. W.; Kawa, S. R.; Kelly, K. K.; Loewenstein, M.; Ferry, G. V.; Chan, K. R.; Gary, B. L. *J. Geophys. Res.* **1992**, *97*, 8015.
(44) Pueschel, R. F.; Ferry, G. V.; Snetsinger, K. G.; Goodman, J.; Dye, J. E.; Baumgardner, D. *J. Geophys. Res.* **1992**, *97*, 8105.
(45) Toon, O.; Browell, E.; Gary, B.; Bait, L.; Newman, P.; Pueschel, R.; Russell, P.; Schoberl, M.; Toon, G.; Traub, W.; Valero, F.; Selkirk, H.; Jordan, J. Submitted for publication in *Science*.
(46) Goodman, J.; Toon, O. B.; Pueschel, R. F. Snetinger, K. G. *J. Geophys. Res.* **1989**, *94*, 16449.
(47) Hanson, D. R.; Ravishankara, A. R. *J. Geophys. Res.* **1991**, *96*, 5081.
(48) Abbatt, J. P. D.; Molina, M. J. *J. Phys. Chem.* **1992**, *96*, 7674.
(49) Leu, M. T.; Moore, S. B.; Keyser, L. F. *J. Phys. Chem.* **1991**, *95*, 7763.